Solid State Ionics 7 (1982) 225–242
North-Holland Publishing Company

LOW-TEMPERATURE IONIC CONDUCTIVITY AND DIELECTRIC RELAXATION PHENOMENA IN FLUORITE-TYPE SOLID SOLUTIONS

K.E.D. WAPENAAR *, H.G. KOEKKOEK
Solid State Department, Physical Laboratory, State University, 3508 TA Utrecht, The Netherlands

and

J. VAN TURNHOUT
Plastics and Rubber Research Institute, T.N.O., P.O. Box 71, 2600 AB Delft, The Netherlands

Received 1 April 1982
Revised manuscript received 18 June 1982

Low-temperature ionic conductivity and dielectric relaxation phenomena in $Ba_{1-x}La_xF_{2+x}$ crystals ($1.19 \times 10^{-3} \leqslant x \leqslant 0.492$) have been studied by ionic thermal current (ITC) and ac dielectric loss (DL) techniques. The conductivity results agree with those of an earlier study of the same crystals at higher temperatures. At low LaF_3 concentrations, i.e. $1.19 \times 10^{-3} \leqslant x \leqslant 2.37 \times 10^{-2}$, the dielectric spectra show three relaxation peaks, two of which are ascribed to simple associates of interstitial F^- ions (F_i') nearest-neighbour (nm) and next-nearest-neighbour (nnn) to substitutional La^{3+} ions (La_{Ba}). They are denoted as type I and II dipoles, respectively. We attribute the third peak to angled ("L-shaped") $\{La_{Ba}2F_i\}'$ complexes. Relaxation parameters for the relaxations are presented. We have calculated effective dipole moments for type I and II dipoles μ_I^{eff} and μ_{II}^{eff}, taking into account the displacements and polarizabilities of the defects. Several combinations of host lattice cations and dopant ions have been considered for the fluorites $M_{1-x}RE_xF_{2+x}$, i.e. M = Ca, Sr, Ba, and RE = La, Eu, Lu. For nearly all combinations the ratio $\mu_{II}^{eff}/\mu_{II}^{eff}$ is found to have a value of 2.4 ± 0.1. With the μ^{eff} values thus obtained, the dipole concentrations of type I and II dipoles can be calculated. Their dependence on solute content is discussed. In the calculations, Debye–Hückel–Lidiard interactions between defects and the charge clouds surrounding them have been taken into account. At high concentrations, i.e. $0.133 \leqslant x \leqslant 0.492$, broad structureless absorption losses dominate the dielectric relaxation spectra. These losses are analysed by the fractional polarization (FP) technique, and by a special analysis of the DL data. The feasibility of these techniques is discussed. The analysis reveals that two localized relaxation processes occur in concentrated solid solutions. One is characterized by reorientation activation enthalpies (ΔH_R) which are the same as the corresponding conductivity activation enthalpies (ΔH), and is ascribed to F-interstitial motion in crystal areas around defect clusters. The second process is characterized by ΔH_R values which are much lower than ΔH. We propose that this process is related to F-interstitial reorientation within clusters. The results presented indicate that no typical polarizable cluster is preferred in concentrated $Ba_{1-x}La_xF_{2+x}$ solid solutions.

1. Introduction

The dielectric properties of alkaline-earth fluorides (MF_2) doped with RE^{3+} fluorides have attracted considerable attention [1–11]. They have recently been reviewed by Crawford [1]. Andeen et al. [2] have conducted dielectric loss (DL) measurements on MF_2 host lattices doped with a variety of RE^{3+} ions.

Dilute solid solutions often show one or two dipole relaxations [6,8]. EPR investigations have shown that these relaxations are due to simple associates of a substitutional RE^{3+} ion ($RE_M^{\cdot}$) and an interstitial fluoride ion (F_i'): a nearest-neighbour (nn) associate having tetragonal symmetry (type I dipole), and a next-nearest-neighbour (nnn) associate having trigonal

* Present address: Plastics and Rubber Research Institute, T.N.O., P.O. Box 71, 2600 AB Delft, The Netherlands.

0 167-2738/82/0000–0000/$ 02.75

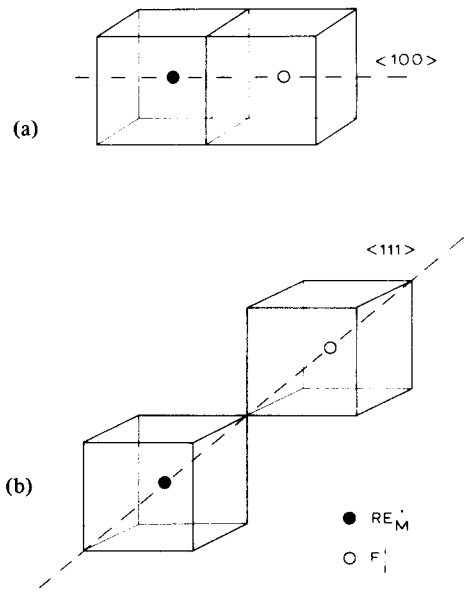

Fig. 1. Type I (a) and type II (b) dipole in the fluorite structure. The tetragonal ⟨100⟩ and trigonal ⟨111⟩ axes are indicated. The corners of the cubes represent the regular anion lattice sites.

symmetry (type II dipole) [12]. Both dipoles are depicted in fig. 1. Whether a type I or a type II dipole, or both will be present in the solid solutions depends critically on the difference between the radii of the host lattice cation and the dopant ion, Δr, as has been shown by lattice simulation calculations [13]. The stability of type I dipoles decreases, while that of type II dipoles increases with Δr.

Spectra showing up to five relaxation peaks have also been reported [2,7]. Laser-selective-excitation investigations [7] have helped to attribute the additional relaxations to F_i' reorientations within polarizable clusters of two or more $RE_M^{\cdot}$ ions and several charge-compensating F_i' ions.

ITC spectra of $Ba_{1-x}La_xF_{2+x}$ solid solutions containing low and moderate dopant concentrations ($10^{-4} < x < 10^{-2}$) show peaks corresponding to type I and II dipoles, and a small third peak ascribed to oxygen in the lattice [3,4]. At high concentrations of dopant, up to $x = 0.26$, the spectra are dominated by a high fourth peak due to the relaxation of macroscopic space charges [5]. This peak shifts to lower temperatures with increasing solute content, which has been related to the decrease of the conductivity activation enthalpy observed in the same concentration region [17].

We recently reported on the ionic conductivity [15], and bulk and interfacial polarization phenomena [16] shown by the $Ba_{1-x}La_xF_{2+x}$ system. We considered LaF_3 concentrations up to the solubility limit in BaF_2, which is about 50 mole% (m/o) [15]. The papers discuss the results of our investigations regarding defect chemical models adequately accounting for the increasing disorder in the solid solutions.

In the study reported here, we investigated the low-temperature dielectric properties of several of these solid solutions by a combination of DL and ITC techniques. To unravel the complicated spectra of concentrated solid solutions, we used novel experimental and data handling methods derived from DL and ITC. Along with a discussion of the results we present an evaluation of these new methods.

2. Experimental details

The growth and characterization of the $Ba_{1-x}La_xF_{2+x}$ solid solution crystals have been described before [15]. Unoriented disks, 1×10^{-3} to 2×10^{-3} m thick, and $\sim 8 \times 10^{-3}$ m in diameter, were cut from the ingots. The large faces of the samples were provided with platinum or gold electrodes. The ITC technique employed to obtain overall and partial relaxation spectra is known as the thermally stimulated polarization current (TSP) technique. In this technique, the sample is cooled to a temperature where the reorientation of the dipoles can be considered as frozen in. The sample is then subjected to a polarizing field and heated at a linear rate, the polarization current being monitored as a function of temperature.

The ITC measurements were performed with a cryostat in which temperatures down to 90 K could be realized in an atmosphere of dry helium. Between 90 and 320 K, the heating rate was about 0.2 K/s. The temperature of the sample was measured with a platinum resistance embedded in one of the electrodes. Polarization currents due to applied fields of 2 to 4 $\times 10^5$ V/m were measured with a Cary 401 vibrating reed electrometer. Current-temperature spectra were recorded with a Bryans 29000 X–Y recorder.

The DL spectra were run with fully automated equipment based on a Solartron 1172 frequency response analyser between frequencies of 1/16 and 32 Hz, and temperatures of 120 and 380 K [55]. Additional DL measurements were conducted between frequencies of 120 Hz to 1 kHz with a General Radio capacitance bridge (706 C), and auxiliary equipment comprising an oscillator, tuned null-detector and balancing capacitors of the same make.

We investigated the effect of thermal treatment on the dielectric spectra of several samples. The samples were first annealed for 12 h at 1250 K in a quartz tube in vacuo (0.1 Pa). Then, they were either slowly cooled (1.1×10^{-3} K/s) or quenched to room temperature.

3. Results and data analysis

The composition of the samples of $Ba_{1-x}La_xF_{2+x}$ investigated was determined by neutron activation analysis [15], and is included in table 1 (samples 1–6). Fig. 2 presents the DL spectra of the six samples at 1 Hz as plots of log ϵ'' versus T. Apart from a number of localized relaxation phenomena, the spectra reveal a contribution of ionic conductivity (σ), which increases with increasing solute content.

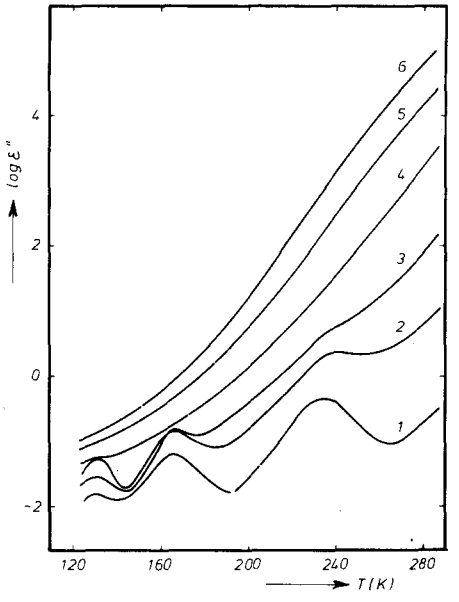

Fig. 2. Dielectric loss of $Ba_{1-x}La_xF_{2+x}$ solid solutions at a measuring frequency of 1 Hz, plotted as log ϵ'' versus T in the temperature region where localized relaxations predominate. The compositions of samples 1–6 (lines 1–6) are presented in table 1.

3.1. Delocalized relaxations: conductivity

At temperatures where the contributions of localized relaxations and space-charge polarization to ϵ'' can be ignored, we have $\epsilon'' = \sigma/\omega\epsilon_0$, where ϵ_0 stands for the permittivity of free space. Together with the well-known expression for the ionic conductivity,

$$\sigma = (A/T)\exp(-\Delta H/kT), \quad (1)$$

the conductivity activation enthalpy (ΔH) can be obtained from a plot of log ωT versus T^{-1}. Values of

Table 1
Compositions in mole fractions (mf), conductivity activation enthalpies (ΔH), and Σ relaxation activation enthalpies (ΔH_R^{Σ}) for the $Ba_{1-x}La_xF_{2+x}$ solid solutions. The techniques used are indicated. See also text.

Sample no.	x (mf)	ΔH (eV)		ΔH_R^{Σ} (eV)	
		DL, TSP	conduct. [15]	DL	DL [16]
1	0.119×10^{-2}	0.92 ± 0.01	0.935 ± 0.010		
2	0.99×10^{-2}	0.775 ± 0.005	0.790 ± 0.017		
3	0.237×10^{-1}	0.69 ± 0.01	0.734 ± 0.010	0.66 ± 0.05	
4	0.133	0.65 ± 0.01	0.671 ± 0.002	0.63 ± 0.04	0.67 ± 0.07
5	0.209	0.61 ± 0.01	0.645 ± 0.006	0.61 ± 0.04	
	0.30 [15]		0.617 ± 0.012		0.57 ± 0.04
	0.448 [15]		0.573 ± 0.008		
6	0.492	0.555 ± 0.005			

ω and T at constant ϵ'' were obtained from plots of ϵ'' versus T for various measuring frequencies. Alternatively, values of ΔH were obtained from TSP measurements. At the voltages applied in these measurements, the platinum or gold electrodes did not block ionic currents. The contribution of the ionic conductivity to the TSP spectra could therefore be measured separately. To this end the localized relaxations are polarized first. The subsequent TSP run in the same polarizing field then yields the non-blocked ionic conduction current [18]. The ΔH values obtained by both techniques are the same within experimental error; their average values are listed in table 1, which also includes the ΔH values obtained in the earlier conductivity study at higher temperatures [15].

3.2. Localized relaxations at low and moderate dopant concentrations

Samples 1–3 show three localized relaxations (see fig. 2). When averaged over a large number of TSP runs, the relaxation peaks, which we have labelled If, I, and II, appear at 121, 147 and 201 K, respectively. Fig. 3 presents the 1 Hz DL and TSP spectra obtained for sample 1, plotted as ϵ'' and σ versus T, respectively. It shows that the two techniques yield comparable results. In fact, an ITC experiment can be regarded as comparable to a DL experiment at an extremely low measuring frequency [19]. The equivalent frequency can be calculated from the temperature at which the peak appears (T_m). Differentiation of the TSP formula [20]

$$j(T) = \frac{N\mu^2 E}{3kT\tau_0} \exp\left\{-\frac{\Delta H_R}{kT} - \frac{1}{b}\int_{T_0}^{T} \frac{1}{\tau(T')}\,dT'\right\} \qquad (2)$$

with respect to the temperature yields

$$\frac{\Delta H_R}{kT_m^2} - \frac{1}{T_m} = \frac{1}{b\tau_m}\,, \qquad (3)$$

where $j(T)$ is the current density at temperature T, N the dipole concentration, μ the dipole moment, E the applied field strength, τ_0 the reciprocal frequency factor, ΔH_R the activation enthalpy for dipole reorientation and b the heating rate. τ_m is the relaxation time at the maximum of the peak and can be obtained from eq. (3) when ΔH_R is known. Since at the peak maximum of a DL measurement the relation $\omega\tau_m = 1$ holds, the equivalent frequency, $\nu = \omega/2\pi$, can be calculated. For the present TSP measurements with b = 0.2 K/s, ν varies from 5 mHz at T_m = 201 K to 7 mHz at T_m = 147 K. Determination of the relaxation parameters ΔH_R and τ_0 from ITC measurements is often hampered by the peak broadening caused by distributions in the relaxation times. Unless this effect is taken explicitly into account in the ITC data analysis ([23], p. 72), [6], reliable "average" values for ΔH_R and τ_0 can only be obtained from DL measurements using peak position data, because such data are not affected by symmetric distributions in τ. Plots of log τ_m versus T^{-1} for the relaxations concerned are presented in fig. 4. In the frequency range

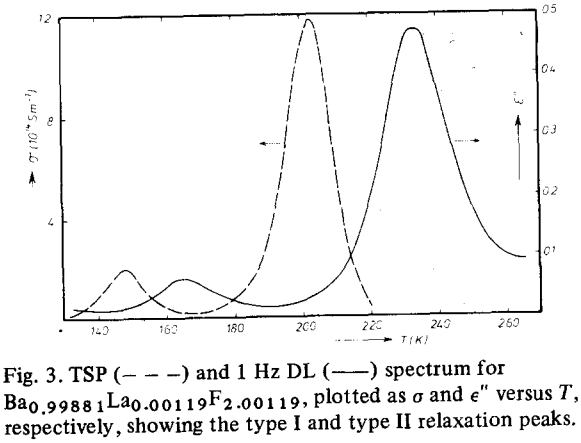

Fig. 3. TSP (– – –) and 1 Hz DL (——) spectrum for $Ba_{0.99881}La_{0.00119}F_{2.00119}$, plotted as σ and ϵ'' versus T, respectively, showing the type I and type II relaxation peaks.

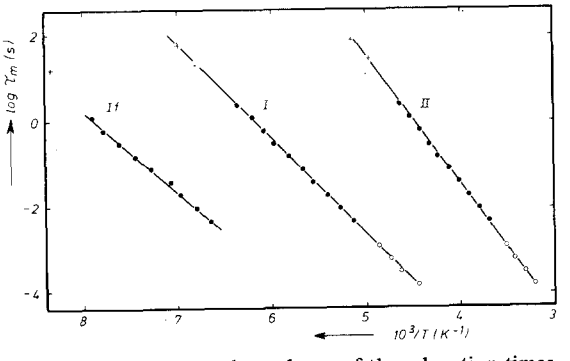

Fig. 4. The temperature dependence of the relaxation times of type If, type I and type II relaxations in $Ba_{1-x}La_xF_{2+x}$, plotted as log τ_m versus T^{-1}. Data are obtained from DL measurements in the frequency ranges: $120 < \nu < 1000$ Hz (○), and $1/16 < \nu < 32$ Hz (●), and from ITC [3] and TSP measurements (+).

120 Hz to 1 kHz the data were obtained on sample 2. In the range 0.063 to 32 Hz average results for the three samples are shown for the relaxations of type I and type II dipoles. Values for much lower frequencies have been calculated from the peak positions of our TSP results, and from the ITC results obtained by Ong and Jacobs [3]. We see that the combination of these experimental techniques yields reliable relaxation time data over a range of about six decades. Owing to the rather low intensity of the If relaxation, reliable results for this relaxation could only be obtained on sample 3. Values for ΔH_R and τ_0 resulting from fig. 4 are presented in table 2, along with values from the literature [3,4]. Dipole concentrations can be calculated from the dielectric strength $\Delta\epsilon = \epsilon_L - \epsilon_H$, according to

$$\Delta\epsilon = N\mu^2/3\epsilon_0 kT. \quad (4)$$

Here ϵ_L and ϵ_H are the low and high-frequency limits of the dielectric constant, low and high being relative to the dispersion produced by the relaxation. Cole–Cole plots (ϵ'' versus ϵ') were employed to determine $\Delta\epsilon$ values for type I and type II relaxations of samples 1–3. Cole and Cole [22] have shown that the depressed arcs commonly seen in the complex-plane representation of the dielectric constant can formally be described by replacing the resistance in the well-known Debye circuit ($R = \tau/\Delta\epsilon$) by a complex impedance: $Z = \bar{\tau}(i\omega\bar{\tau})^{-\beta}/\Delta\epsilon$. Here $\bar{\tau}$ stands for the average relaxation time, and β can be regarded as a distribution parameter related to the width of a distribution in relaxation times. Incidentally, it has recently been shown [16] that a frequency-dependent element of this form is frequently invoked in the modeling of frequency dispersions in the small-signal ac response of various electrolytes. The analytical expression for the complex dielectric constant ϵ^* then reads

$$\epsilon^* = \epsilon_H + \frac{\Delta\epsilon}{1 + (i\omega\bar{\tau})^{1-\beta}}. \quad (5)$$

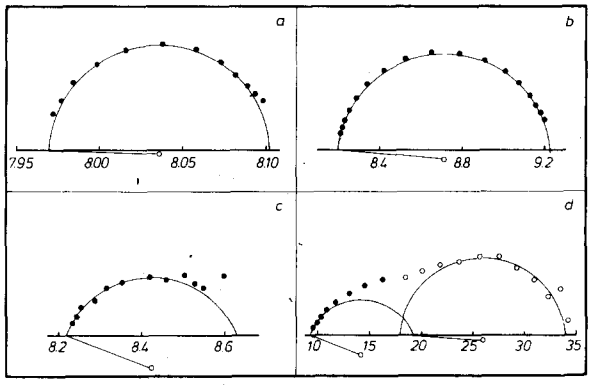

Fig. 5. Cole–Cole plots (ϵ'' versus ϵ') for type I (a, c) and type II (b, d) dipoles in $Ba_{0.99881}La_{0.00119}F_{2.00119}$ (a, b) and $Ba_{0.9763}La_{0.0237}F_{2.0237}$ (c, d). The vertical axes (ϵ'') of the plots have been omitted for the sake of clarity. According to convention, the scales of the axes are the same as those of the corresponding horizontal axes. Parameters obtained from these plots are included in table 3. See also text.

In the experimental setup used the number of data points obtained for ϵ' and ϵ'' as a function of temperature at one measuring frequency is much higher than that obtained as a function of frequency at a fixed temperature. We therefore used the temperature dependencies $\epsilon'(T)$ and $\epsilon''(T)$ of the 1 Hz measurements to construct Cole–Cole-type plots with T as the measuring parameter. These plots are presented in fig. 5. In view of eq. (5) the experimental values of $\epsilon'(T)$

Table 2
Relaxation parameters for several relaxations in $Ba_{1-x}La_xF_{2+x}$, presented as ΔH_R (eV) and $-\log \tau_0$ (s). Values for $-\log \tau_0$ are in parentheses. The symbols are explained in the text.

Ref.	If	I	Ox	II
[4]		0.39 ± 0.02 (12.3 ± 0.7)		0.50 ± 0.02 (11.5 ± 0.5)
[3]		0.391 (12.0)	0.492 (14.5)	0.544 (12.2)
present results	0.454 ± 0.010 (14.1 ± 0.2)	0.430 ± 0.003 (13.55 ± 0.02)		0.595 ± 0.003) (13.45 ± 0.03)

and $\epsilon''(T)$ need to be corrected for the temperature dependencies $\epsilon_H(T)$ and $\Delta\epsilon(T)$. For the first correction, $\epsilon_H(T)$ is assumed to be dominated by the temperature dependence of the static dielectric constant, $\epsilon_s(T)$. In the relevant temperature regions, the variations in $\epsilon_s(T)$ are approximated by linear interpolations of the $\epsilon_s(T)$ data reported by Wintersgill et al. [21]: $d\epsilon_s/dT = 1.375 \times 10^{-3}$ K^{-1} ($140 < T < 180$ K), and $d\epsilon_s/dT = 1.475 \times 10^{-3}$ K^{-1} ($220 < T < 260$ K). This first correction (Fc) only applies to ϵ' (see eq. (5)), and can be written:

$$\epsilon'(T_e + \Delta T)_{Fc} = \epsilon'(T_e + \Delta T) - (d\epsilon_s/dT)\Delta T. \quad (6)$$

T_e is the temperature at which $\epsilon''(T)$ reaches its maximum. The second correction, $\Delta\epsilon(T)$ (see eq. (4)), applies to both ϵ' and ϵ'', and is taken into account as follows:

$$\epsilon'(T_e) = \epsilon_H(T_e) + (\epsilon'(T_e + \Delta T)_{Fc} - \epsilon_H(T_e)) \times (T_e + \Delta T)/T_e \quad (7a)$$

and

$$\epsilon''(T_e) = \epsilon''(T_e + \Delta T)\frac{T_e + \Delta T}{T_e}. \quad (7b)$$

Fig. 5. reveals that the data thus obtained adequately fit depressed arcs. The values for T_e and the values obtained for $\Delta\epsilon$ and β are presented in table 3. It should be noted that the data presented in fig. 5d were obtained by subtraction of an appreciable contribution of ionic conductivity from the ϵ'' data. The conductivity contribution was calculated by extrapolation of a fit of high-temperature ϵ'' data to the conductivity equation, eq. (1). The additional relaxation on the high-temperature side of the type II relaxation of sample 3, shown in fig. 5d (o), is not observed in samples 1 and 2 (see below).

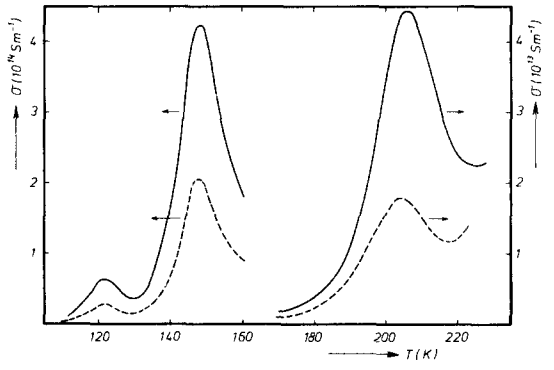

Fig. 6. Effect of high-temperature annealing followed by slow cooling on the TSP spectrum of $Ba_{0.9901}La_{0.0099}F_{2.0099}$: —— as grown, – – – after thermal treatment. With increasing temperatures the spectra reveal the presence of type If, type I and type II relaxation peaks.

To conclude the results for samples 1–3, we show (fig. 6) the effect on the TSP spectrum of sample 2 of annealing at a high temperature followed by slow cooling. High-temperature annealing followed by rapid cooling to room temperature (quenching) almost restores the peak intensities to their original (as grown) values.

3.3. Localized relaxations at high dopant concentrations

Fig. 2 shows that for samples 4–6, log ϵ'' increases smoothly with temperature. This is owing to the ionic

Table 3
Effective temperatures T_e, dielectric strengths $\Delta\epsilon$, and Cole–Cole distribution parameters β for the Cole–Cole plots (fig. 5) of type I and type II dipoles in samples 1–3. Included are calculated values of N_I, N_{II}, the ratio N_{II}/N_I, and the percentage of defects present in the dipoles

Sample	Dipole	T_e (K)	$\Delta\epsilon$	β	N $\times 10^{-25}$ (m^{-3})	N_{II}/N_I	[Dipoles] (%)
1	I	165.5	0.133	0.98	0.63	1.90	91
	II	233	1.035	0.94	1.20		
2	I	165.5	0.331	0.90	1.57	4.91	56
	II	240.5	6.42	0.81	7.71		
3	I	172	0.41	0.80	2.0	5.7	33
	II	240	9.5	0.76	11.4		

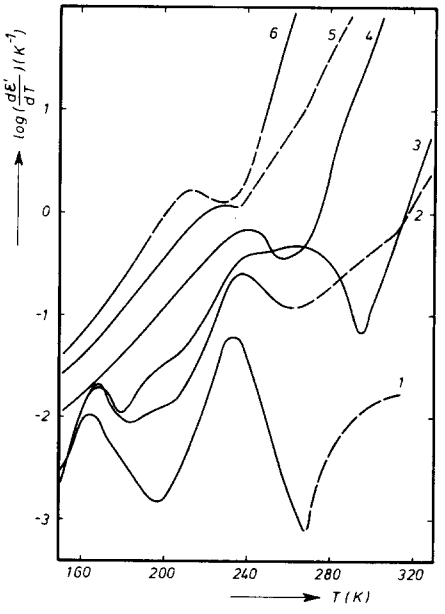

Fig. 7. Dielectric loss of $Ba_{1-x}La_xF_{2+x}$ solid solutions, plotted as log $d\epsilon'/dT$ versus T. The compositions of samples 1–6 (lines 1–6) are presented in table 1. The broken lines indicate those parts of the spectra that are less reliable owing to wide scatter of the data points (sample 6), or to electrode–electrolyte contact problems (samples 1, 2 and 5).

conductivity contributing significantly to the dielectric spectra even at relatively low temperatures. Unlike fig. 2, a better separation between localized phenomena (dipole relaxation) and delocalized ones (ionic conductivity) is obtained when, instead of log ϵ'', log $d\epsilon'/dT$ is plotted versus T [23]. This is done for all six samples in fig. 7, which shows a clear separation between localized and delocalized events. The relaxation located between the type II relaxation and the conduction loss, which was also observed in the Cole–Cole plot of sample 3 (compare fig. 5d), now comes clearly to the fore. This relaxation, which will be referred to as a type Σ relaxation, gradually shifts to lower temperatures with increasing solute content of a sample, and it is the only one observed separately in samples 4–6. Values of ΔH_R for the type Σ relaxation have been estimated from plots of log τ_m versus T^{-1}, and are presented in table 1. The reciprocal frequency factors lie between 10^{-15} and 10^{-14} s.

The shape of the TSP spectra of samples 4–6 is similar to that of the log ϵ'' versus T spectra. The

Table 4
Relaxation parameters ΔH_R (eV) and $-\log \tau_0$ (s) from the FP spectra of $Ba_{0.791}La_{0.209}F_{2.209}$ (fig. 8). Values for $-\log \tau_0$ are in parentheses

a	0.15 (6.2)	*d*	0.24 (7.8)	*g*	0.42 (12.1)
b	0.15 (5.3)	*e*	0.28 (8.9)	*h*	0.45 (12.6)
c	0.21 (7.3)	*f*	0.35 (10.5)	*i*	0.62 (cf. table 1)

broad absorption loss at the low-temperature side of the spectrum of sample 5 has further been analysed by the fractional polarization (FP) technique. With this technique, which is closely related to other thermal sampling (TS) techniques [19], a broad absorption can be tested for the presence of a distribution in relaxation activation enthalpies. To this end, a number of TSP spectra are recorded, each spectrum being started at a higher polarization temperature. Values of ΔH_R are calculated from the initial rising currents in the spectra, and the corresponding frequency factors are obtained from eq. (3). For T_m a temperature is chosen near the middle of the reciprocal temperature region where the current increases exponentially. In this procedure it is assumed that the initial rise of each partial spectrum is dominated by a single relaxation process. The results of the FP measurements are shown in fig. 8, and the values obtained

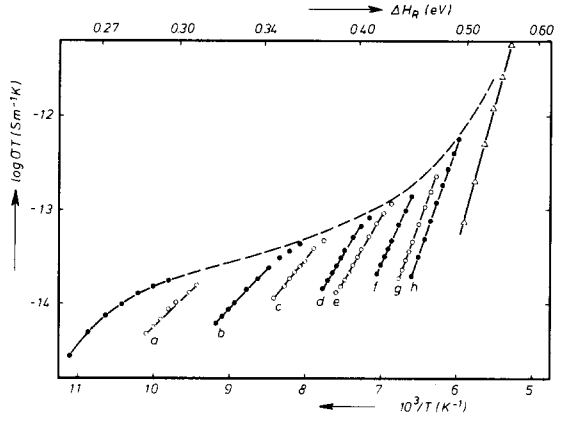

Fig. 8. FP spectra for $Ba_{0.791}La_{0.209}F_{2.209}$, plotted as log σT versus T^{-1}. Values for ΔH_R obtained from the slopes of these curves are presented in table 4. The broken line represents the overall TSP spectrum of this sample. The upper axis is explained in the text (section 4.4). Line *i* represents the ionic conductivity.

for ΔH_R and τ_0 are collected in table 4. The upper axis in fig. 8 will be explained in section 4.4.

Alternatively, the variation of an "apparent" relaxation activation enthalpy, ΔH_R^*, can be obtained from DL measurements by a method suggested by Solunov and Ponevski [24]. These authors showed that, when the temperature dependence of ϵ' or ϵ'' is measured for at least two frequencies, it is possible to obtain a plot of log τ versus T^{-1} spanning a wide range of relaxation times. The method is based on the relation

$$\omega_1\tau(T_0) = \omega_2\tau(T_1), \tag{8}$$

which is valid if one takes equal products of ϵ'' and T for different frequencies, see fig. 9. It follows from the expressions for ϵ''. For instance,

$$\epsilon''(\omega, T) = \Delta\epsilon(T)\,\frac{\omega\tau(T)}{1+\omega^2\tau^2(T)} \tag{9}$$

for a single relaxation time. It has been shown [24] that relation (8) also holds for distributions of relaxation times. If eq. (8) represents the first "step" of equal $\epsilon''T$, a second step of equal $\epsilon''T$ is started at T_1, see fig. 9

$$\omega_1\tau(T_1) = \omega_2\tau(T_2). \tag{10}$$

Combining eqs. (8) and (10), we get $\tau(T_2) = (\omega_1/\omega_2)^2\tau(T_0)$. For the nth step, we obtain

$$\tau(T_n) = (\omega_1/\omega_2)^n\tau(T_0) \tag{11}$$

and for ΔH_R^* in the temperature interval $T_0 - T_n$, as derived from eq. (11), we find

$$\Delta H_R^* = 2.303\,k\,\frac{n\log\omega_1/\omega_2}{(1/T_n - 1/T_0)}. \tag{12}$$

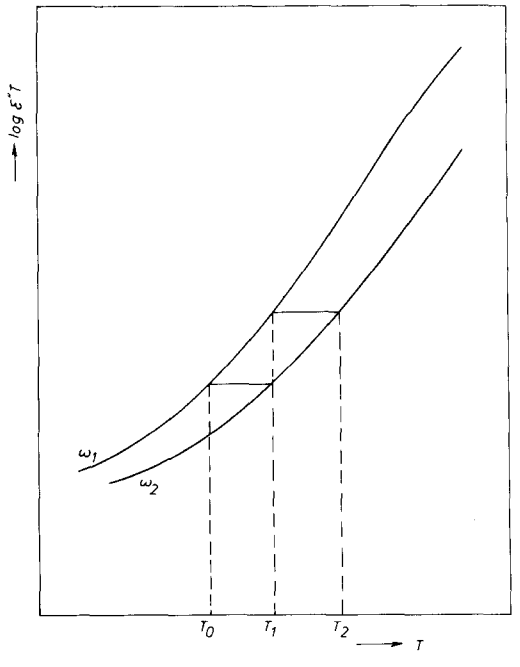

Fig. 9. Schematic illustration of the method suggested by Solunov and Ponevski [24] to obtain the temperature dependence of a relaxation activation enthalpy from measurements at two frequencies. (See text.)

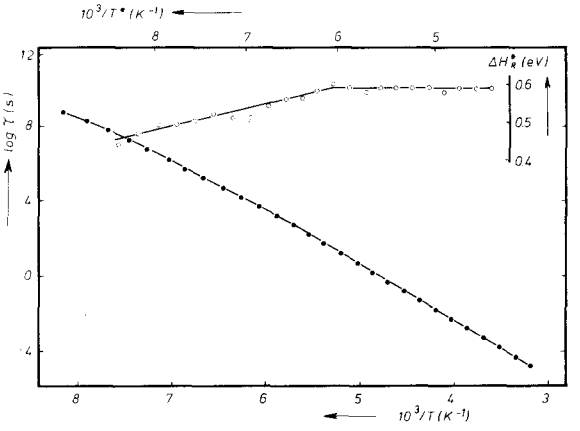

Fig. 10. Temperature dependence of the relaxation time for $Ba_{0.791}La_{0.209}F_{2.209}$ obtained by the method of Solunov and Ponevski [24], plotted as log τ versus $10^3/T$. The temperature dependence of ΔH_R^*, obtained from the slope of the plot, is also shown. The upper $10^3/T^*$ axis is explained in the text.

Fig. 10 is a plot of log τ versus T^{-1} for sample 5. The data for this plot were obtained from $\epsilon''T$ versus T^{-1} curves measured at five frequencies, with an average frequency of 1 Hz (0.1 Hz $< \nu <$ 10 Hz). The log τ axis has been scaled with the value $\tau_0 = 5 \times 10^{-15}$ s. The τ values obtained span a range of almost 14 decades. ΔH_R^* values were calculated from eq. (12), sets of 5 successive log $\tau(T)$ values being taken. They are included in fig. 10. We calculated the upper temperature axis in fig. 10 ($10^3/T^*$) with eq. (8), using the average measuring frequency (1 Hz), and the equivalent ITC frequency (~6 mHz), in order

to make it easier to compare the DL and FP results (fig. 8).

4. Discussion

In this section we shall examine the implications of the results of the measurements. The discussion is divided into four sections successively dealing with ionic conductivity, simple associates, the type If relaxation, and broad absorption losses.

4.1. Ionic conductivity

ITC studies usually point up a tall high-temperature peak that shifts to lower temperatures with increasing solute content [4,5]. Laredo et al. [4] ascribed this peak to relaxations of the charge cloud surrounding dislocations. However, by using the TSP technique with non-blocking electrodes, and by combining TSP and conductivity measurements [25], one of us has shown that the relaxation is due to ionic conductivity.

In a recent paper [15], we have discussed the ionic conduction properties of $Ba_{1-x}La_xF_{2+x}$ solid solution crystals in detail. Its main conclusions are summarized below, and related to the results presented here. The dependence of conductivity on composition falls into three concentration regions [15]:

(i) $x < 10^{-3}$.

In this region there are free defects and associates between $La^{\bullet}_{Ba}$ and F'_i defects. ΔH is composed of the free F'_i activation enthalpy for motion, $\Delta H_{m,F'_i}$, and the association activation enthalpy, ΔH_A, such that

$$\Delta H = \Delta H_{m,F'_i} + \tfrac{1}{2}\Delta H_A$$

with the numerical values $\Delta H_{m,F'_i} = (0.714 \pm 0.003)$ eV and $\Delta H_A \approx 0.39$ eV.

(ii) $1 \times 10^{-3} < x \lesssim 5 \times 10^{-2}$.

In the "intermediate" concentration region, the changes in conductivity and ΔH are the most drastic. A rapid increase of the conductivity is accompanied by a large drop in ΔH (compare table 1). This effect has been ascribed to the decrease of ΔH_A with increasing solute content which the Debye–Hückel–Lidiard (DHL) theory [26] attributes to defect–defect interactions. As this theory will be applied in a different context below, we present its essential features. As is well known, the theory of ideal solutions is not applicable to (solid) solutions containing moderate dopant concentrations ($x \geqslant 10^{-3}$), because it ignores Coulombic interactions between defects. Lidiard [26] therefore applied to ionic solids the theory of Debye and Hückel for nonideal electrolyte solutions. According to this theory, the association enthalpy is lowered by the interaction energy between the free defect and the charge cloud surrounding it [26]:

$$\Delta H_A = \Delta H_A^0 - \frac{q^2\kappa}{4\pi\epsilon\epsilon_0(1+\kappa R)}, \tag{13}$$

where

$$\kappa = \left(\frac{2q^2x_c}{v\epsilon\epsilon_0 kT}\right)^{1/2}. \tag{14}$$

Here κ represents the Debye–Hückel screening constant, R the distance of closest approach for free defects, v the volume per molecule of BaF_2, and x_c the concentration of free charged defects. The other parameters have their usual meanings.

Relations (13) and (14) reveal that an increasing solute content will lead to a decrease of ΔH_A. Consequently, the free F'_i concentration, and hence the ionic conductivity, will increase rapidly. A comparison of the ΔH (DL, TSP) values with the ΔH (conduct.) values (table 1) reveals a slight increase of ΔH with average measuring temperature. This result is in line with eqs. (13) and (14), because the free F'_i concentration increases exponentially with temperature, and so contributes to a further decrease of ΔH_A.

In the limit of the DHL description ($\Delta H_A = 0$), F interstitials jump from interstitial positions in neutral associates to interstitial positions near uncompensated $La^{\bullet}_{Ba}$ defects, thus contributing to the conductivity without affecting the association equilibrium. This conduction mechanism is the one that prevails in the third concentration region:

(iii) $x \gtrsim 5 \times 10^{-2}$.

In this region of high concentrations, the conductivity increases exponentially, and ΔH decreases linearly. These effects are accounted for in the enhanced ionic motion (EIM) model: The large number of lattice-disturbing defect clusters causes the conduction mechanism to be governed by a broad distribution of defect jumps with slightly different activation en-

thalpies. If the distribution function is assumed to be a Gaussian one, the conductivity equation reads [15]:

$$\sigma T = A_0 \exp\left\{-\frac{1}{kT}\left(\overline{\Delta H}_m - \frac{p^2}{4kT}\right)\right\}, \quad (15)$$

the conductivity activation enthalpy being given by

$$\Delta H = \overline{\Delta H}_m - \frac{p^2}{2kT}, \quad (16)$$

where $\overline{\Delta H}_m$ is the average value of ΔH, and p the width of the distribution function. Eq. (16) also indicates a slight increase of ΔH with average measuring temperature, as is observed here (compare table 1).

We conclude that the results obtained here for the low-temperature conductivity confirm the previously reported interpretations of conductivity results obtained at higher temperatures [15].

4.2. Simple associates

In this section we discuss the type I and type II dipoles, which have been identified [3,4] as simple nn and nnn associates of $La^{\bullet}_{Ba}$ and F'_i defects, respectively (fig. 1). Ong and Jacobs [3] have pointed out that the attribution of the higher relaxation peak (type II) to nnn associates is substantiated by the EPR spectra of $BaF_2 : Gd^{3+}$ [27,28] and $BaF_2 : Yb^{3+}$ [29], which are dominated by a trigonal spectrum. However, lattice simulation calculations [13] have shown that the results for $BaF_2 : Gd^{3+}$ and $BaF_2 : Yb^{3+}$ cannot be extended to $BaF_2 : La^{3+}$. The relative stabilities of nn and nnn associates, which determine the predominance of one of these dipoles, depend critically on the difference Δr between the ionic radii of the host lattice cation and the RE^{3+} ion. For instance, the calculations successfully predict the switch from predominantly nn to predominantly nnn associates that is seen in $SrF_2 : RE^{3+}$ [6] with increasing Δr. The calculations indicate a similar change-over in $BaF_2 : RE^{3+}$ for RE^{3+} ions smaller than Ce^{3+}. In addition, the EPR spectrum reported for $BaF_2 : Ce^{3+}$ is tetragonal [30].

A more convincing argument for the proposed attribution, also pointed out by Ong and Jacobs [3], is found in the similarity between the activation enthalpy for the reorientation of type II dipoles in $BaF_2 : La^{3+}$, and that for the only relaxation observed in the TSP spectrum of $BaF_2 : Tb^{3+}$ [18]. Since the ionic radii of Tb^{3+} and Gd^{3+} are almost the same, it is no doubt correct to attribute this relaxation to nnn associates. Similarly, the attribution of the type I dipole to nn associates has been based on a comparison with results for $CaF_2 : RE^{3+}$ [3].

The same assignments are used here, and throughout this section it will be shown that these assignments lead to consistent results. We would emphasize, however, that resolving existing contradictory results for the $BaF_2 : Ce^{3+}$ system needs a combination of dielectric and EPR measurements. In the following we discuss the relaxation parameters ΔH_R and τ_0, the dipole moments μ, and the composition dependence of the dipole concentrations $N(x)$, for the type I and type II dipoles.

4.2.1. ΔH_R and τ_0

The values of ΔH_R and $-\log \tau_0$ we obtained in this investigation for the type I and type II dipoles are higher than those reported in the literature (compare table 2). The former are probably more reliable, because they were determined by a technique that is insensitive to peak broadening effects.

The entropy for reorientational motion, ΔS_R, can be estimated from the values obtained for τ_0. Using the notation of Matthews and Crawford [9], we can write for the relaxation times for type I and type II dipoles

$$\tau^{I} = 1/4w_{11}, \quad \text{and} \quad \tau^{II} = 1/3w_{21}, \quad (17)$$

where w_{ij} represents the jump frequency from site i to site j, and the subscripts 1 and 2 refer to an nn and nnn site, respectively. Since $w_{ij} = \nu_a \exp(-\Delta G_R/kT)$, we obtain the relations

$$\Delta S^{I}_R = -k \ln 4\nu_a \tau^{I}_0 \quad (18a)$$

and

$$\Delta S^{II}_R = -k \ln 3\nu_a \tau^{II}_0, \quad (18b)$$

where ν_a is the attempt frequency. Incidentally, Andeen et al. [10] arrived at the expression $\Delta S^{II}_R = -k \ln 2\nu_a \tau^{II}_0$ for a type II relaxation in $SrF_2 : Er^{3+}$. The factor of 2 in this expression results when a direct nnn → nnn jump is assumed for the type II relaxation, whereas a factor of 3 in eq. (18b) applies to a situation where this dipole reorients via an nn site [31], which

is not unlikely (see e.g. fig. 3c in ref. [9]).

Taking for ν_a the zone-centre transverse-optical mode, $\nu_a = \nu_{TO} = 5.67 \times 10^{12}$ s^{-1} [32], we find entropy values of $(0.45 \pm 0.05)k$ and $(0.50 \pm 0.07)k$ for ΔS_R^I and ΔS_R^{II}, respectively. These values are much lower than the ones reported for the motion of free F_i' ions in BaF_2, viz. $\Delta S_{m,F_i'} \simeq (4.45 - 5.1)k$ [33]. The decrease of ΔS, when going from free to bound F_i' motion, qualitatively correlates with the corresponding decrease of ΔH.

In fact, such a relation between ΔH and ΔS is to be expected (see also section 4.4). Those reported τ_0 values for the type I and type II relaxations which have been obtained from ITC spectra (table 2) all lead to large negative values for ΔS_R, indicating that they are often too high owing to the aforementioned peak broadening effects.

4.2.2. Dipole moments

From the $\Delta\epsilon$ values obtained for the type I and type II dipoles it is possible by means of eq. (4) to calculate the dipole concentrations, provided that correct values of μ_I and μ_{II} are known. The dipole moments for defect pairs in an ionic crystal are usually calculated with the unrelaxed-point-ion (UPI) model: $\mu_I = qa$, and $\mu_{II} = qa\sqrt{3}$, where q is the electronic charge and a the shortest anion–anion separation in the fluorite structure. Lidiard [34] has pointed out that the Lorentz internal field factor for point dipoles, $(\epsilon_s + 2)/3$, does not apply to extended dipoles, and that a correction to the UPI values is likely to be small. Several authors [9,11,35] have shown, however, that the ratio between μ_{II} and μ_I in SrF_2 is larger than $\sqrt{3}$. Reported values are 2.4 [9], $\geqslant$2.8 [11], and 2.32 [35].

For this reason, Aalbers and Den Hartog [35] proposed to calculate μ by a model that takes into account the deformation of the host lattice, as well as the electronic polarizabilities of the nearest F-lattice ions and the defects. In this polarizable-point-ion (PPI) model an effective dipole moment μ_{eff} is calculated for the two defects and the nearest F-lattice ions, both placed in a spherical cavity surrounded by a dielectric continuum. As proposed by Onsager [36], they multiplied the resulting dipole moment by a factor of $3\epsilon_s/(2\epsilon_s + 1)$. Using electronic polarizabilities for $SrF_2 : La^{3+}$, and approximate ionic displacements for $CaF_2 : Ce^{3+}$, they arrived at the value 2.28 for the ratio $\mu_{II}^{eff}/\mu_I^{eff}$ in SrF_2 [35].

The main objection against this method is the arbitrariness of the cavity size. Aalbers and Den Hartog used a cavity including only ions for which the polarization yields a negative contribution on the effective dipole moment, viz. for the type I dipole the four central F-lattice ions and the two defects (see fig. 1). Taking a smaller or a larger cavity drastically affects the results of the calculations. We therefore present a different approach here.

In a recent study Wapenaar and Catlow [13] have calculated association energies in RE^{3+}-doped alkaline-earth fluorides, using computational methods based on the Mott–Littleton method. In this method a large number of ions, constituting and surrounding the defect configuration of interest, are explicitly displaced from their normal lattice sites until the configuration of minimum energy is obtained. The displacements of the defects, $\delta_{RE_M^\bullet}$ and $\delta_{F_i'}$, resulting from the calculations with a "semi-empirical" set of potentials [13], are employed in the present evaluation of μ_I and μ_{II}. Values for $\delta_{RE_M^\bullet}$ and $\delta_{F_i'}$ relative to the unrelaxed $RE_M^\bullet - F_i'$ separations are presented in table 5. A positive value of δ means that the defect is displaced along the symmetry axis of the dipole towards the oppositely charged defect. As in the UPI method, the electronic polarizations and displacements of the lattice ions are ignored. For a first approximation this is reasonable, because the effects on the lattice sites largely cancel out owing to the symmetry of the lattice. A more rigorous calculation, however, will have to take the perturbation of the symmetry into account. The relaxed-polarizable-point-ion (RPPI) model we present here, takes into account three contributions to the effective dipole moment μ^{eff}. The first is the dipole moment of the relaxed dipole,

$$\mu_1 = (1 - \delta_{RE_M^\bullet} - \delta_{F_i'})\mu, \tag{19}$$

where μ represents the UPI value. The second arises from the displacement of the RE^{3+} ion from its normal lattice site. A dipole with an effective charge $2q$ and a length $\delta_{RE_M^\bullet}$ results:

$$\mu_2 = -2\delta_{RE_M^\bullet}\mu. \tag{20}$$

The third arises from the electronic polarizability of the F_i' ion, plus the difference in electronic polarizability between the RE^{3+} ion and the lattice cation. The following values for the polarizabilities were used

Table 5
Defect ion displacements [13] and effective dipole moments for type I and type II dipoles in $M_{1-x}RE_xF_{2+x}$. The ratios $\mu_{II}^{eff}/\mu_I^{eff}$ are to be compared with the ratio $\mu_{II}/\mu_I = 1.73$. (See also text.)

		Type I dipoles			Type II dipoles			$\mu_{II}^{eff}/\mu_I^{eff}$
		$\delta_{RE_M^{\cdot}}$	$\delta_{F_i'}$	μ_I^{eff}/μ_I	$\delta_{RE_M^{\cdot}}$	$\delta_{F_i'}$	μ_{II}^{eff}/μ_{II}	
CaF_2:	La	0.043	0.044	0.731	−0.015	0.017	1.013	2.40
	Eu	0.048	0.059	0.697	−0.013	0.029	0.994	2.47
	Lu	0.051	0.064	0.681	−0.012	0.040	0.980	2.49
SrF_2:	La	0.054	0.069	0.703	−0.012	0.035	0.991	2.44
	Eu	0.058	0.074	0.685	−0.010	0.049	0.970	2.45
	Lu	0.051	0.042	0.543	−0.009	0.063	0.953	2.22
BaF_2:	La	0.052	0.087	0.733	−0.009	0.051	0.972	2.30
	Eu	0.057	0.112	0.691	−0.009	0.061	0.962	2.41
	Lu	0.011	−0.027	0.977	−0.008	0.070	0.950	1.68

[37]: $\alpha_F = 1.04 \times 10^{-30}$ m^3, and $\alpha_{La} - \alpha_M = 0.57$, 0.18 and -0.51×10^{-30} m^3 for M = Ca, Sr and Ba, respectively.

$$\mu_3 = -\mu[\alpha_F + (\alpha_{La} - \alpha_M)]/l^3(1 - \delta_{RE_M^{\cdot}} - \delta_{F_i'})^2, \quad (21)$$

where $l = a$ for a type I dipole, and $l = a\sqrt{3}$ for a type II dipole. Values calculated for μ^{eff} ($= \mu_1 + \mu_2 + \mu_3$), for type I and type II dipoles and for various MF_2 : RE^{3+} combinations are presented in table 5 as μ^{eff}/μ.

These results reveal that the assumption $\mu_{II}^{eff} \simeq \mu_{II}$ is quite reasonable, whereas μ_I^{eff} is considerably smaller than μ_I. The short distance between the defects in the type I dipole clearly causes larger ionic displacements and larger electronic polarization, which lead to the low value of μ_I^{eff} obtained. The ratio $\mu_{II}^{eff}/\mu_I^{eff}$ is remarkable constant for the MF_2 : RE^{3+} combinations considered here, and has an average value of 2.4 ± 0.1, in agreement with experimental results for SrF_2 [9,35]. Interestingly, values for this ratio smaller than 2.4, and even smaller than $\sqrt{3}$, can be expected for a large host lattice with a small dopant ion, e.g. BaF_2 : Lu^{3+} (see table 5). This is due to large inward displacements of the four central F-lattice ions in the type I dipole in such a system. Consequently, the F interstitial is repelled, which leads to a relatively large value for μ_I^{eff}.

On the basis of the employed RPPI model, we conclude that the relations: $\mu_{II}^{eff} \simeq \mu_{II}$, and $\mu_I^{eff} \simeq 0.72\,\mu_I$ apply to most MF_2 : RE^{3+} combinations.

4.2.3. Dipole concentrations

Now that the values for the dipole moments are known, the dipole concentrations for type I and type II dipoles can be calculated by means of eq. (4). The results are collected in table 3, together with the relative amount of dopant present in the simple associates. Table 3 shows that this amount decreases with increase ing solute content, which is in line with the conclusion arrived at in the conductivity study on $Ba_{1-x}La_xF_{2+x}$ crystals (see section 4.1). The tendency to form associates decreases with increasing solute content owing to defect–defect interactions. In addition, it is well known that, in alkaline-earth fluorides, La^{3+}, Y^{3+} and RE^{3+} ions tend to aggregate and form defect clusters of various configurations (see, e.g., ref. [38]). Obviously, cluster formation also restricts the amount of defects available for the formation of simple associates.

The Cole–Cole distribution parameter β, also included in table 3, decreases with increasing solute content, and $\beta_{II} < \beta_I$. Since β is related to the width of a distribution in the relaxation times [22] (the smaller the value for β, the broader the distribution function), the compositional dependence of β reflects the increasing disorder with solute content. The influence of the disorder on the type II dipole is more pronounced, since the nnn associate is larger than the nn associate.

Table 3 further reveals that the concentration ratio between type II and type I dipoles strongly depends on the solute content. The same behaviour has been

reported by Aalbers and Den Hartog [35] for N_{II}/N_I in $SrF_2 : Gd^{3+}$. These authors reported an increase of the ratio N_{II}/N_I from ~0.097 to ~0.44 at a temperature of 200 K and in the concentration range $2.1 \times 10^{-4} < x < 1.6 \times 10^{-3}$. A practically concentration-independent ratio between the ITC peak heights of type II and type I relaxations has, by contrast, been reported for $Ba_{1-x}La_xF_{2+x}$ ($10^{-4} < x < 10^{-2}$) [3,4]. However, care should be taken in determining dipole concentrations from peak heights. For instance, the method employed by Laredo et al.. [4] ignores the effect of peak broadening. This problem is avoided when the dipole concentration is determined from the area under the peak, or from a Cole–Cole plot. It is unlikely, however, that peak broadening alone can account for the observed discrepancy between our results and the literature data [3,4].

Laredo et al. [4] use their observation of a concentration-independent ratio of peak heights as additional support for assigning the peaks to simple associates in thermal equilibrium. That this is a questionable conclusion follows from the work of Aalbers and Den Hartog [35], and is further demonstrated here. The relative stability of type I and type II associates depends on the difference of their association free energies ΔG_{12} ($= \Delta H_{12} - T\Delta S_{12}$):

$$\frac{N_{II}}{N_I} = \exp\left(\frac{\Delta S_{12}}{k} - \frac{\Delta H_{12}}{kT}\right). \tag{22}$$

The entropy and enthalpy differences are denoted as $\Delta S_{12} = \Delta S_{A,II} - \Delta S_{A,I}$ and $\Delta H_{12} = \Delta H_{A,II} - \Delta H_{A,I}$, where $\Delta S_{A,i}$ and $\Delta H_{A,i}$ represent the association entropy and enthalpy, respectively, for a type i dipole. Assuming $\Delta S_{12} = 0$ [9] over the entire solute range, we can calculate ΔH_{12} values from the values obtained for the ratio N_{II}/N_I. Table 6 lists ΔH_{12} values for $T = 200$ K, the temperature at which the equilibrium between type I and type II dipoles can be regarded as frozen in.

Table 6
Difference in association enthalpy ΔH_{12} between type II and type I dipoles, free defect concentrations calculated with the DHL interaction theory, and the resulting relative amount of defects present in clusters

Sample	ΔH_{12} (meV)	x_c (mf)	[Clusters] (%)
1	11	1.1×10^{-4}	–
2	27	2.4×10^{-3}	20
3	30	3.2×10^{-3}	53

Aalbers and Den Hartog [35] have shown that an increase of ΔH_{12} with solute content can be accounted for by a distributed nature of $\Delta H_{A,I}$ and $\Delta H_{A,II}$. As $\Delta H_{A,II}$ broadens more rapidly than does $\Delta H_{A,I}$, ΔH_{12} increases with solute content.

We present here an approach based on the defect–defect interactions described in the DHL theory (compare section 4.1). We recall that ΔH_A decreases with increasing solute content owing to the electrostatic interactions between the free defects and their surrounding charge clouds. This holds irrespective of whether one considers $\Delta H_{A,I}$ or $\Delta H_{A,II}$. Therefore, ΔH_{12} can be modified by means of eq. (13) and the appropriate values of the distances of closest approach (R), i.e. $R = a\sqrt{3}$ for the nn associate and $R = a\sqrt{5}$ for the nnn associate. The resulting relation for ΔH_{12} reads:

$$\Delta H_{12} = \Delta H_{12}^0 + \frac{q^2}{4\pi\epsilon\epsilon_0}\left\{\frac{1}{a\sqrt{3} + \kappa^{-1}} - \frac{1}{a\sqrt{5} + \kappa^{-1}}\right\}, \tag{23}$$

where ΔH_{12}^0 ($= \Delta H_{A,II}^0 - \Delta H_{A,I}^0$) represents the enthalpy difference in an interaction-free lattice (i.e. a very dilute solution).

To illustrate the implications of this model, we calculate the free defect concentration x_c from eqs. (14) and (23). The parameter ΔH_{12}^0 is calculated from data obtained on sample 1, under the assumption that x_c equals the difference between the nominal impurity concentration and the dipole concentration in this sample. The screening constant κ is calculated for $T = 200$ K, i.e. the temperature employed in the calculation of ΔH_{12}. The value obtained for ΔH_{12}^0 is 8 meV, the values for x_c in mole fractions (mf) being included in table 6. The relative amounts of defects present in defect clusters are calculated from the nominal concentration of defects (table 1), the total concentration of dipoles (table 3), and the concentration of free defects, and are also listed in table 6. This reveals that the x_c values obtained from the model presented are quite reasonable in comparison with the nominal defect concentrations and dipole

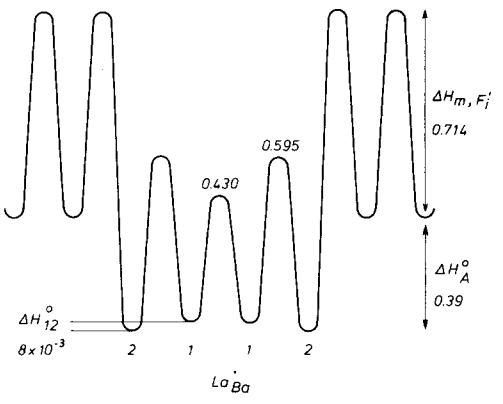

Fig. 11. Schematic illustration representing several activation enthalpies occurring in dilute $Ba_{1-x}La_xF_{2+x}$ solid solutions. The values are in eV. 1 and 2 represent the nn and nnn F-interstitial positions, respectively.

concentrations. The values for x_c do not exceed 1×10^{-2} mf, which has been found to be the upper limit for the free defect concentration in $Ba_{1-x}La_xF_{2+x}$ solid solutions [15]. In addition, the resulting amount of defects present in defect clusters increases superlinearly with solute content, as is to be expected.

To conclude this section on the type I and the type II dipoles, fig. 11 schematically presents several activation enthalpies applying to a $Ba_{1-x}La_xF_{2+x}$ crystal free of defect–defect interactions.

4.3. Type If relaxation

The ITC spectra of $Ba_{1-x}La_xF_{2+x}$ reported by Ong and Jacobs [3] reveal a third relaxation on the high-temperature side of the type I relaxation. These authors attributed this relaxation, labelled type Ox in table 2, to the presence of O_F'–$V_F^{\bullet}$ associates. The absence of this relaxation in our TSP and DL spectra (fig. 3) indicates that our samples contain little oxygen as an impurity.

On the low-temperature side of the type I relaxation, the spectra of our samples show another relaxation, labelled If (fig. 2). This relaxation was not seen in the reported ITC studies on $Ba_{1-x}La_xF_{2+x}$ [3,4], because it appears at temperatures outside the ranges covered in those studies. To investigate the nature of the complex giving rise to this relaxation, we treated several samples thermally.

Laredo et al. [4] found that high-temperature annealing followed by slow cooling erased all traces of the type I and type II relaxation peaks from the ITC spectra for $Ba_{1-x}La_xF_{2+x}$. Fig. 6 shows the effect of a similar treatment on the TSP spectrum of sample 2. The intensities of the three relaxation peaks have decreased.

At high temperatures, close to the melting point, the mobility of the cations allows formation or dissolution of aggregates of cations of the dopant. Since defect clusters are more stable than simple associates [43], cations of the dopant will continue to aggregate upon cooling until their mobility is frozen in. Therefore, high-temperature annealing followed by slow cooling will reduce the concentration of simple associates, whereas that of clusters will be increased. High-temperature annealing followed by quenching will have the opposite effect. The results of thermal treatment of the present samples indicate that the three relaxations must be assigned to simple associates (fig. 6).

Crawford and Matthews [39] have suggested that the presence of $\{RE_M 2F_i\}'$ complexes in fluorite-type crystals accounts for the anomalously high concentration of isolated $RE_M^{\bullet}$ defects in these crystals. They propose that the $\{RE_M F_i\}^x$ associate acts as a trap for F_i' defects:

$$\{RE_M F_i\}^x + F_i' \rightleftharpoons \{RE_M 2F_i\}'. \qquad (24)$$

This trapping mechanism has been extended by Tallant et al. [40] to include scavenging of F_i' defects by dimers $\{2RE_M 2F_i\}^x$ and trimers $\{3RE_M 3F_i\}^x$ in $CaF_2 : Er^{3+}$. Catlow et al. [41] and Jacobs and Ong [42] have calculated that the most stable configuration of the $\{RE_M 2F_i\}'$ complex is the L-shaped one, with the two F_i' defects occupying nn interstitial sites. This configuration is more stable than a linear F_i'–$RE_M^{\bullet}$–F_i' complex, because it derives additional stability from similar F-lattice ion displacements, such as are observed in the 222 clusters [43]. The L-shaped $\{RE_M 2F_i\}'$ complex has a net dipole moment, and the ΔH_R value for the reorientation of this dipole may well be lower than $\Delta H_{R,I}$, because the F-lattice ion involved in the interstitialcy jump is already displaced towards an interstitial position. In addition, the trapping equilibrium [24] shows that the concentration of these dipoles depends on the concentration of simple associates. The peak height of the re-

laxation related to $\{RE_M 2F_i\}'$ complexes will, therefore, depend on thermal treatment in a way similar to that anticipated for type I and type II dipoles.

Summarizing the arguments set forth above, we feel justified in assigning the type If dipole to the L-shaped $\{La_{Ba} 2F_i\}'$ complex.

4.4. Broad absorption losses

The samples containing high concentrations of solute (samples 4–6) show only one maximum in a plot of log ($d\epsilon'/dT$) versus T (fig. 7). Sample 3 shows the same maximum in the corresponding Cole–Cole plot (fig. 5d). This relaxation, labelled Σ, has been noted before in a study of the small-signal ac response of concentrated $Ba_{1-x}La_xF_{2+x}$ solid solutions [16]. In the temperature region $300 < T < 350$ K, the frequency responses of crystals with compositions x = 0.133 and x = 0.30 were fitted to an equivalent circuit consisting of a non-Debye circuit parallel to the bulk conductivity, the Cole–Cole plots representing the data thus obtained revealed an absorption loss with a low value for the Cole–Cole distribution parameter, viz. $\beta \simeq 0.4$. The values obtained for the relaxation parameters ΔH_R and τ_0 compare well with the values obtained here for the type Σ relaxation (see table 1).

Table 1 further reveals that the ΔH_R values for the type Σ relaxation are the same as the corresponding values of the conductivity activation enthalpies ΔH. This implies that the lattice distortions around F-interstitials contributing to the type Σ relaxation, and those around F-interstitials contributing to the ionic conductivity, are the same. As we mentioned in the previous section, Tallant et al. [40] have proposed a defect model for fluorites in which several more or less extended clusters can scavenge F-interstitials. The motion of these interstitials is confined to an area around the cluster (type Σ relaxation), unless the interstitial can jump into a site where it is bound to a neighbouring cluster (conductivity through percolation). The intensity of the type Σ relaxation increases with solute content (fig. 7). This means that the number of F-interstitials bound to clusters, or the areas around the clusters, or both, increase with solute content.

As in section 4.4.1, it is possible to estimate the entropy for reorientational motion for the type Σ relaxation. If we assume that the jump takes place in only one direction, ΔS_R^Σ reads (compare eq. (18)):

$$\Delta S_R^\Sigma = -k \ln \nu_a \tau_0^\Sigma . \tag{25}$$

With $\tau_0^\Sigma = 10^{-14}$–10^{-15} s (section 3), ΔS_R^Σ is calculated to be $(4.0 \pm 1.1)k$.

This value compares well with the entropy values reported for the motion of free F_i' defects in BaF_2, viz. $\Delta S_{m,F_i'} = 4.4$–5.1 [33], which agrees with the proposed relaxation mechanism.

On the low-temperature side of the DL and TSP spectra, the intensity of the absorption loss decreases only slightly with temperature (compare fig. 8). Here, the results of the FP experiment on sample 5 (table 4) indicate the presence of a distribution of relaxation processes with ΔH_R values much lower than ΔH (conductivity). The values of ΔH_R^* obtained from the DL measurements by the method of Solunov and Ponevski [24] (see fig. 10) lead to the same conclusion, because they also decrease with temperature. Before going into a possible relaxation mechanism for these broad absorption losses with low ΔH_R values, we will discuss the feasibility of the methods employed.

When the relaxation parameters obtained from the FP curves (table 4) are plotted as log τ_0 versus ΔH_R, they are found to obey the "compensation law":

$$\tau = \tau_c \exp\left\{\frac{\Delta H_R}{k}\left(\frac{1}{T} - \frac{1}{T_c}\right)\right\}. \tag{26}$$

This behaviour is frequently observed in TS experiments [44–47]. The data obtained here lead to $\tau_c = (7 \pm 6) \times 10^{-3}$ s, and $T_c = 213 \pm 9$ K. In polymers the compensation temperature T_c has been related to the glass transition temperature [44,45], whereas in apatites it has been related to a phase transition from monoclinic to hexagonal symmetry [46].

Alternatively, eq. (26) has been used to obtain a relation between ΔH_R and ΔS_R [47]. With $\tau = (n\nu_a)^{-1} \exp(\Delta G_R/kT)$, where n is the symmetry number of the reorientation, eq. (26) yields:

$$\Delta H_R = T_c \Delta S_R + \Delta H_c . \tag{27}$$

Here ΔH_c is a constant, and stands for $kT_c \ln n\nu_a\tau_c$. Linear relations between the enthalpy and entropy have in fact been proposed for temperature-activated processes in inorganic [48,49] and polymeric solids [50]. In these relations T_c is related to the reciprocal

isobaric volume coefficient of thermal expansion (α), i.e. $T_c \simeq 1/4\alpha$ and $\Delta H_c = 0$ for inorganic solids [48] (for a recent more detailed account, see ref. [51]). For polymeric solids $T_c = 1/9\Delta\alpha$ and $\Delta H_c = \Delta H_{tor}$, where $\Delta\alpha$ is the difference in α between the rubbery and glassy state, ΔH_{tor} representing an internal torsional enthalpy [50].

Zielinski et al. [47] interpreted their TS results on polymethyl methacrylate (PMMA) using eq. (27). Their data satisfactorily reproduced the expected value for $\Delta\alpha$ in polymers, but the negative values for ΔS_R they obtained seem difficult to interpret. From our results we obtain for α a value of 1.2×10^{-3} K^{-1}, which differs markedly from that reported for nominally pure BaF_2, viz. $\alpha = 5.37 \times 10^{-5}$ K^{-1} [52]. These interpretations of TS results therefore seem questionable.

At this stage we recall that the analysis of ITC results with the conventional one-relaxation-time formulas (e.g. eq. (2)) often leads to ΔH_R and $-\log \tau_0$ values being underestimated owing to peak broadening. Zielinski et al. [47] explicitly report that in their study of PMMA each TS peak was broadened! We therefore conclude that the observed compensation behaviour is inherent to the experimental technique in question, and that the values of ΔH_R and $-\log \tau_0$ listed in table 4 are too low, owing to the peak broadening effect of distributions, even in the case of the sampled spectra.

Since activation enthalpies deduced from ac dielectric loss measurements are less prone to the effects of distributions, the method of Solunov and Ponevski [24] is to be preferred for obtaining "apparent" values of ΔH_R (ΔH_R^*) at several temperatures (see fig. 10). ΔH_R is called apparent because it represents an average value for two or more overlapping relaxation processes. Fig. 10 reveals that ΔH_R^* is temperature-independent, i.e. $\Delta H_R^* = 0.59$ eV, for $T > 190$ K. The corresponding curves for sample 5 in figs. 2 and 7 indicate that at these temperatures, the dielectric response is dominated by the ionic conductivity ($\Delta H = (0.60 \pm 0.01)$ eV) and by the type Σ relaxation ($\Delta H_R^{\Sigma} = (0.61 \pm 0.02)$ eV). The agreement between the enthalpy values is satisfactory. For $T < 190$ K, ΔH_R^* decreases, indicating a new relaxation process with a lower activation enthalpy, or a distribution in ΔH_R values. Our results do not allow a more detailed analysis of the DL data, along lines proposed by Solunov and Ponevski [24]. A comparison of ΔH_R values obtained by the FP technique (table 4) with ΔH_R^* values (fig. 10, upper $1/T^*$ axis) reveals that $\Delta H_R^* > \Delta H_R$ for corresponding temperatures, as is expected from the peak broadening effects. Combining the DL and FP results, we conclude that on the low-temperature side of the spectra ($T < 190$ K), a relaxation process characterized by a distribution in ΔH_R values predominates.

One of us has shown (eq. (3.58)) in ref. [19]) that the shape of a distribution $P(\Delta H_R)$ is to a first approximation similar to that of the corresponding ITC spectrum. If $P(\Delta H_R)$ is to be obtained from $I(T)$, a relation between ΔH_R and T is required. This relation should result from TS or FP experiments. However, because these techniques do not provide reliable values of ΔH_R, we decided to use eq. (3), assuming a constant value for τ_0, viz. $\tau_0 = 10^{-13.4}$ s, which is the average value of τ_0 for type I and type II relaxations. The resulting ΔH_R values are presented on the upper axis in fig. 8, and the broken line in this figure now represents a plot of $\log P(\Delta H_R)$ versus ΔH_R for ΔH_R values in the range 0.30–0.45 eV. The spectrum is truncated at $\Delta H_R \simeq 0.30$ eV owing to the limited temperature range in the experiments.

As the most likely relaxation process that accounts for a broad distribution with rather low ΔH_R values, we suggest the reorientation of defects within clusters. From a comparative study of the DL spectra of a variety of RE^{3+} ions in CaF_2, SrF_2 and BaF_2, Andeen et al. [2] concluded that the tendency for cluster formation decreases with increasing size of the host-lattice cation. Using the results of lattice simulation calculations reported by Catlow [43,53], Schoonman and Wapenaar [54] arrived at the same conclusion. The absence of a clear-cut maximum in the distribution function we found indicates that, in fact, there is no preferred polarizable cluster in $Ba_{1-x}La_xF_{2+x}$. However, final confirmation has to wait for dielectric measurements at temperatures below 90 K.

Summarizing the dielectric properties of the concentrated $Ba_{1-x}La_xF_{2+x}$ solid solutions, we conclude that three processes can be discerned:

(i) Ionic conductivity on the high-temperature side of the spectra;

(ii) Localized F-interstitial motion in crystal areas around clusters at intermediate temperatures;

(iii) Defect reorientations within the clusters at low temperatures.

Finally, we suggest that fluorite-type solid solutions like $Ba_{1-x}La_xF_{2+x}$ samples form an ideal model system for studying the dielectric properties of disordered compounds (ionic solids, glasses, polymers), because the disorder in these solutions can be gradually increased.

Acknowledgement

We thank Mr. P.J.M. van den Heuvel and Mr. P.J. Droppert for assistance in the experimental work, Dr. J. Schoonman and Professor G. Blasse for critically reading the manuscript, and for encouraging this investigation, and Mr. G.P.M. Léger for correcting the English.

References

[1] J.H. Crawford, Impurity-Defect Dipole Reorientation in Alkaline Earth Fluorides, presented at the Symposium on Physics of Condensed Matter (Caracas, 1980).
[2] C.G. Andeen, J.J. Fontanella, M.C. Wintersgill, P.J. Welcher, R.J. Kimble and G.E. Matthews, J. Phys. C14 (1981) 3557.
[3] S.H. Ong and P.W.M. Jacobs, J. Solid State Chem. 32 (1980) 193.
[4] E. Laredo, M. Puma and D.R. Figueroa, Phys. Rev. B19 (1979) 2224.
[5] H.W. den Hartog, Dielectric Experiments on Concentrated Solutions of $XF_2 : R^{3+}$. EPS Meeting, Solid State Division (Antwerp, 1980); Proceedings (Plenum Press, New York, 1981), in press.
[6] W. van Weperen and H.W. den Hartog, Phys. Rev. B18 (1978) 2857.
[7] J. Fontanella, D.J. Treacy and C. Andeen, J. Chem. Phys. 72 (1980) 2235.
[8] N. Kristianpoller and Y. Kirsh, J. Phys. C12 (1979) 1073.
[9] G.E. Matthews and J.H. Crawford, Phys. Rev. B15 (1977) 55.
[10] C. Andeen, L.M. Hayden and J. Fontanella, Phys. Rev. B21 (1980) 794.
[11] J. Fontanella, D.L. Jones and C. Andeen, Phys. Rev. B18 (1978) 4454.
[12] J.M. Baker, in: Crystals with the fluorite structure, ed. W. Hayes (Clarendon, Oxford, 1974) p. 341.
[13] K.E.D. Wapenaar and C.R.A. Catlow, Solid State Ionics 2 (1981) 245.
[14] R.H. Nafziger and N. Riazance, J. Am. Ceram. Soc. 55 (1972) 130.
[15] K.E.D. Wapenaar, J.L. van Koesveld and J. Schoonman, Solid State Ionics 2 (1981) 145.
[16] K.E.D. Wapenaar and J. Schoonman, Solid State Ionics 2 (1981) 253.
[17] J. Schoonman, Solid State Ionics 5 (1981) 71.
[18] C. Hong and D.E. Day, J. Appl. Phys. 58 (1979) 5352.
[19] J. van Turnhout, in: Topics in Appl. Phys. 33: Electrets, ed. G.M. Sessler (Springer, Berlin, 1978) p. 81.
[20] S.W.S. McKeever and D.M. Hughes, J. Phys. D8 (1975) 1520.
[21] M. Wintersgill, J. Fontanella, C. Andeen and D. Schuele, J. Appl. Phys. 50 (1979) 8259.
[22] K.S. Cole and R.A. Cole, J. Chem. Phys. 9 (1941) 341.
[23] J. van Turnhout, Thermally stimulated discharge of polymer electrets (Elsevier, Amsterdam, 1975) p. 224.
[24] Ch. Solunov and Ch. Ponevski, J. Polym. Sci. 14 (1976) 1801.
[25] K.E.D. Wapenaar, J. Phys. (Paris) 41 (1980) C6-220.
[26] A.B. Lidiard, in: Handbuch der physik, ed. S. Flügge (Springer, Berlin, 1957) p. 246.
[27] J. Sierro, Phys. Letters 4 (1963) 178.
[28] C.A. Batner, R.W. Reynolds and M.M. Abraham, J. Chem. Phys. 52 (1970) 1248.
[29] W. Ranon and A. Yaniv, Phys. Letters 9 (1964) 17.
[30] A. Kiel and W.B. Mims, Phys. Rev. B 6 (1972) 34.
[31] A.S. Nowick, Adv. Phys. 16 (1967) 1.
[32] P. Denham, G.R. Field, P.L.R. Morse and G.R. Wilkinson, Proc. Roy. Soc. A 317 (1970) 55.
[33] P.W.M. Jacobs and S.H. Ong, Crystal Lattice Defects 8 (1980) 177.
[34] A.B. Lidiard, in: Crystals with the fluorite structure, ed. W. Hayes (Clarendon, Oxford, 1974) p. 150.
[35] A.B. Aalbers and H.W. den Hartog, Phys. Rev. B19 (1979) 2163.
[36] L. Onsager, J. Am. Chem. Soc. 58 (1936) 1486.
[37] C. Kittel, Introduction to solid state physics (Wiley, New York, 1976) p. 441.
[38] J. Schoonman, in: Fast ion transport in solids, eds. P. Vashishta, J.N. Mundy, G.K. Shenoy (North-Holland, Amsterdam, 1979) p. 631.
[39] J.H. Crawford and G.E. Matthews, Semicond. Insulators 2 (1977) 213.
[40] D.R. Tallant, D.S. Moore and J.C. Wright, J. Chem. Phys. 67 (1977) 2897.
[41] C.R.A. Catlow, J.D. Comins, F.A. Germano, R.T. Harley and W. Hayes, Phys. Letters 71A (1979) 97.
[42] P.W.M. Jacobs and S.H. Ong, J. Phys. Chem. Solids 41 (1980) 431.
[43] C.R.A. Catlow, J. Phys. C9 (1976) 1859.
[44] D. Chatain, P. Gautier and C. Lacabanne, J. Polymer Sci., Polym. Phys. Ed. 11 (1973) 1631.
[45] C. Lacabanne, D. Chatain, J.C. Monpagens, A. Hiltner and E. Baer, Solid State Commun. 27 (1978) 1055.
[46] N. Hitmi, D. Chatain, C. Lacabanne, J. Dugas, J.C. Trombe, C. Rey and G. Montel, Phys. Status Solidi (a) 60 (1980) 501.
[47] M. Zieliński, T. Świderski and M. Kryszewski, Polymer 19 (1978) 883.

[48] R.W. Keyes, J. Chem. Phys. 29 (1958) 467.
[49] A.W. Lawson, J. Phys. Chem. Solids 3 (1957) 250.
[50] S. Isoda and K. Asai, J. Appl. Phys. (Japan) 13 (1974) 1333.
[51] P. Varotsos, D. Kostopoulos and S. Mourikis, Phys. Status Solidi (a) 57 (1980) 331.
[52] A.C. Bailey and B. Yates, Proc. Phys. Soc. (London) 91 (1967) 390.
[53] C.R.A. Catlow, J. Phys. C 9 (1976) 1845.
[54] J. Schoonman and K.E.D. Wapenaar, J. Electrochem. Soc. 126 (1979) 1385.
[55] J. van Turnhout and K.E.D. Wapenaar, to be published.